AIAA-2001-0517

# Supersonic Pulsed Injection

A. D. Cutler, G. C. Harding
The George Washington University, JIAFS,
Hampton, VA

G.S. Diskin
NASA Langley Research Center, Hampton, VA

**39th AIAA Aerospace Sciences Meeting and Exhibit**

8-11 January 2001 / Reno, NV

AIAA-2001-0517

# HIGH FREQUENCY SUPERSONIC PULSED INJECTION

A. D. Cutler*, G. C. Harding†
*The George Washington University, JIAFS, Hampton, VA*
G. S. Diskin‡
*NASA Langley Research Center, Hampton, VA*

## ABSTRACT

An injector has been developed to provide high-speed high-frequency (order 10kHz) pulsed injection in a supersonic crossflow. The injector nozzle is formed between the fixed internal surface of the nozzle and a freely rotating 3- or 4-sided wheel embedded within the device. Flow-induced rotation of the wheel causes the nozzle throat to open and close at a frequency proportional to the speed of sound of the injected gas. Measurements of frequency and mass flow rate as a function of supply pressure are discussed for various injector designs. Preliminary results are presented for wall-normal injection of helium into a Mach-2 ducted airflow. The data include schlieren images in the vicinity of injection and images of the injectant plume in a plane normal to the flow, downstream of injection.

## NOMENCLATURE

| | |
|---|---|
| $a^*$ | sonic speed of sound |
| $A^*$ | effective sonic throat area |
| $A_{plume}$ | plume cross-sectional area |
| $A_{throat}$ | fixed nozzle minimum area |
| $f$ | pulsation frequency |
| $h$ | duct height (38.61 mm) |
| $K$ | threshold coefficient |
| $\dot{m}$ | injector mass flow rate |
| $N_0, N_1, N_2$ | pixel values |
| $p$ | pressure |
| $p_{duct}$ | duct inlet pressure (105±2 kPa) |
| $p_{exit}$ | injector exit pressure |
| $p_t$ | injector inlet pressure |
| $t$ | time |
| $\Delta A_{plume}$ | standard deviation of $A_{plume}$ |
| $\gamma$ | ratio of specific heat capacities |
| $\rho^*$ | sonic density |
| $\tau$ | pulsation period ($1/f$) |

## INTRODUCTION

Fuel-air mixing is one of the critical problems of scramjet design. Short mixing distances permit short combustors, minimizing engine weight, surface friction and heat transfer. Devices intended to increase the rate of mixing of an injected fuel jet, and that act at the point of injection, may loosely be broken down into two categories according to the magnitude of the disturbance: (1) those producing small perturbations, and (2) those producing large disturbances.

Devices in the first category must depend in their action on exciting natural instabilities of the jet near the point of injection. Such devices have proven effective in enhancing mixing in, say, supersonic turbojet afterburners[1], but have proven to be ineffective in scramjet flows[2,3,4]. For most practical injectors (e.g., wall jets and ramp injectors), mixing is dominated by the formation (rollup) of a counterrotating pair of streamwise vortices, and the effects of even relatively large perturbations are small in comparison. For example, the effects of jet swirl and skew on mixing, while large in the vicinity of injection, were found to be small downstream (but still well upstream of complete mixing), when comparisons were made on a basis of equal injectant pressure and mass flow rate.[5,6,7]

Devices in the second category may be effective in increasing mixing by strengthening or otherwise favorably altering the mechanism of formation of the vortex pair. Ramp injectors do this simply by means of their geometry, but at the expense of device drag. An alternative approach, proposed by Bogdanoff[8] and Seiner et al.[9], is to use pulsed injection. Pulsed injection has proved effective in increasing jet mixing and penetration in subsonic flows[10]. The idea is that the dominant mixing mechanism of steady injection, that of

---

*Associate Professor, Senior Member AIAA

†Graduate Research Scholar Assistant, Student Member AIAA

‡Research Scientist, Senior Member AIAA

longitudinal-vortex-roll-up, be replaced by the mechanism of vortex ring rollup. Thus, at the start of an injection cycle, a vortex would form at the interface between injectant and air. This vortex would grow during injection, detach from the surface as a ring at the end of the injection cycle, and then convect downstream. Repeated injection cycles would lead to a continuous stream of downstream traveling vortex rings.

However, the situation is more complicated in supersonic flow. Steady supersonic injectors, whether flush-wall angled jets, or whether ramp injectors, create a bow shock that is important in the formation and rollup of the dominant longitudinal vortex pair. Indeed, the bow shock or ramp usually creates a boundary-layer separation, lifting boundary-layer vorticity away from the wall, and bow-shock curvature may create significant vorticity[11]. On the other hand, supersonic pulsed injection would create an unsteady system of bow shocks and time-dependent patterns of vorticity via unsteady separations and curved shocks. These competing effects may change the relative performance of pulsating versus non-pulsating injectors in a manner depending on geometry.

Very little previous work has been conducted on the topic of pulsed injection into supersonic flow. Vakili et al.[12] built a small free piston shock tube to study a single jet pulse into a supersonic cross flow. Although the data were very limited, there appeared to be qualitative similarities between the supersonic and previously studied subsonic flows. Seiner[9] presents preliminary results of a numerical simulation of pulsed injection from the base of a ramp that imply a modest increase in mixing with little loss in total pressure. Given the complexity of the problem, and the little previous work, a detailed fundamental investigation of the various phenomena involved would seem to be required.

Clearly, pulsation frequency is a very important parameter in any study of pulsed injection. A target "center" frequency, about which frequency should be varied, may be estimated by assuming that the distance traveled by the airstream in the duct (the approximate streamwise length of the vortex-ring structures) is of the order of the spanwise dimension of the stream tube of air with which the injected fuel is to be mixed. A much lower frequency, say less that $1/10^{th}$, would result in a quasi-steady flow field in which the flow would be the same as steady injection at that instantaneous injection rate. A much higher frequency, say greater that 10 times, would result in small-scale structures that merge together long before mixing is complete. It would also produce a steady bow shock (if this is important).

The above criteria lead to very high pulsation frequencies (perhaps in the range 10-50 kHz). Thus the initial problem in any investigation of pulsed injection is to design an injector. Mechanical valves would seem to be too slow. Bogdanoff[8] proposed in some detail a fluidic device based on the Hartmann-Sprenger tube, but this device does not seem to have been built and tested.

The current work reports on the development of a pulsed injector and the first results for injection into a supersonic crossflow.

## FLOW APPARATUS

The experiment was conducted in the Transverse Jet, a small free jet facility located at the NASA Langley Research Center. This facility consists of a plenum, supplied with high-pressure (unheated) air from a central compressor station, and containing an acoustic damper and flow conditioning screens. In the present experiment the (total) pressure of the air provided to the model was 793±8 kPa. Mounted upon the plenum is a rectangular convergent-divergent nozzle, with exit cross-section 87.88 mm by 38.61 mm and exit Mach number of 1.975±0.01. Thus, the nominal pressure of the flow entering the duct, $p_{duct}$, is 105±2 kPa. On top of this nozzle is mounted a constant area duct incorporating the injector, as shown in Figure 1. The exit of the duct is open to the laboratory (the flow is nominally at atmospheric pressure) and the flow discharges into an overhead exhaust duct. Helium was supplied to the injector from high-pressure cylinders.

The target injector pulsation frequency for this experiment, calculated utilizing the duct height (38.61 mm) as the (stream tube) dimension and an air stream velocity of 514 m/s, was 13.3 kHz. Thus, the injector designed for this study should ideally provide frequencies over a range from several times smaller than 13.3 kHz to several times larger, or if it is to be at least useful, some significant portion of this range. The injector concept of Bogdanoff [8] is in principle capable of frequencies in the desired range, but was dismissed, perhaps prematurely, in favor of a mechanical flow-driven valve concept. It was thought that the latter would be less risky and require less development, although in the end significant development work was involved.

The pulsed injector is illustrated in Figure 2. It consists of an "insert" which is 5.08 mm thick, into which flow passages and a raceway for a rotating wheel

are cut. The insert is clamped between two "blocks", which close the passages from the side. The wheel is nominally 5.03 mm thick, and from each side protrudes a shaft, onto which bearings are pressed. The bearings are of a conventional nature and available with either steel or ceramic balls. For steel balls they are rated to 140,000 RPM, but are capable of some unspecified higher speed with ceramic balls. Ceramic balls were utilized, and the bearings were successfully operated to 240,000 RPM for short periods. The bearings fit in recesses in the blocks so that the wheel rotates freely. Machining tolerances are tight, with the clearance between the wheel and each block in the range 0.025-0.05 mm. The wheel is statically balanced to 50 μinches.

Flow from the injectant supply bottles enters the supply passage in the insert through a hole in one of the blocks and impinges upon the upper surface of the wheel, inducing anti-clockwise rotation. Flow exits the device through the gap between the wheel and the insert.

## METHOD

### Injector Development

The injection development studies were conducted with both air and helium, and with discharge into stagnant air. Seven insert and three wheel geometries, in various combinations, were investigated. The initial combination was a square wheel and an insert with a constant area inlet passage (Wheel 1, Insert 1, shown in Figure 3). The frequency for this combination was not high enough, so additional inserts and wheels were designed and tested in order to gain insight into the important design parameters, and iterate toward the required frequencies. Selected results are reported for Inserts 1, 5, 6, 7 and Wheels 1, 3 using the insert/wheel designations of Harding[13]. Further details are given in this reference.

Mean pressure measurements utilized strain-gauge type pressure transducers, with ±0.5% uncertainty, and temperatures utilized thermocouples with ±2 K uncertainty. A helium-neon laser beam was pointed at the wheel, and the scattered light was detected with a photomultiplier tube (pmt). The signal thus obtained was roughly sinusoidal and, in conjunction with an oscilloscope, could be used to measure frequency (±2%) or to trigger other experiments. Injector volumetric flow rate was measured with a turbine flow meter mounted in a section of constant area pipe. Pressure and temperature measurements were required to obtain mass flow rate. The setup was calibrated to a "standard" nozzle, with uncertainty in mass flow rate of ±2%.

Data acquired include measurements of pulsation frequency and mass flow rate as a function of inlet passage pressure and gas. For geometrically similar devices, the pulsation frequency or mass flow rate is expected to be a function of the inlet passage pressure, the pressure into which the jet discharges, the gas supply temperature, the gas constant and ratio of specific heat capacities, and some characteristic length of the device. It is assumed that viscosity and bearing friction are negligible. With four dimensions (mass, length, time, temperature), the problem can be expressed as follows:

$$\frac{fL}{a^*}, \frac{\dot{m}}{\rho^* a^* L^2} = F\left(\frac{p_t}{p_{exit}}, \gamma\right)$$

Since $L$ is constant in these tests, frequency results are simply plotted in terms of $f/a^*$ ($m^{-1}$), where $a^*$ is nominally 317 m/s for air and 883 m/s for helium, and $p_{exit}$ is nominally 101 kPa. (The target pulsation $f/a^*$, assuming helium injection into the duct flow, is 13,300/883=15.1 $m^{-1}$.) Mass flow results are plotted in terms of sonic area:

$$A^* = \frac{\dot{m}}{\rho^* a^*}$$

Here, $\rho^*$ and $a^*$ are calculated assuming isentropic flow to Mach 1 from measured inlet conditions.

Pressure time histories were obtained for the Insert 7 cases with a miniature, high-frequency-response (nominal natural frequency of 840 kHz), silicon-diaphragm, strain-gauge pressure transducer. The transducer was embedded in the insert with its pressure-sensitive surface flush, as seen in Figure 1.

In certain cases, surface flow within the injector was visualized simply by the flow of grease originating in the bearings, which was dusted with lamp-black.

Digitized images of the flow near the exit of the injector were obtained with a spark schlieren system, a video camera, and a PC with frame grabber. These images were synchronized to selected phases of injection by time delaying the trigger pulse from the oscilloscope, and using it to trigger the schlieren light source.

### Injection into Duct Flow

Only three injector configurations were considered in the study of helium injection into the duct flow, all utilizing Insert 7. Injector inlet pressures were $p_t/p_{duct}$=16.4 and 32.7. The first configuration utilized no wheel, providing steady sonic injection from the

fixed nozzle in the insert. The second utilized Wheel 1, providing pulsed injection at 4.6 kHz and 5.1 kHz respectively, and the third utilized Wheel 3, providing pulsed injection at 11.8 kHz and 12.8 kHz respectively. Unfortunately, frequencies greater than the target frequency (13.3 kHz) were not possible. Schlieren images were not acquired for the Insert 7 Wheel 3 case since it was initially believed that the bearings would fail at the projected wheel rotation speed.

Images were obtained of the flow near the exit of the injector with the spark schlieren system. The duct sidewalls were replaced with windows for this experiment.

Cross-sectional images of the helium plume at the exit of the duct were obtained by imaging Rayleigh scattering from a laser light sheet. In this technique, ethanol is evaporated into the helium supply at a rate (very roughly) of 100 parts per million. The ethanol, once expanded (and cooled) in the injection process, condenses in the flow to form of order-of-magnitude 50 nm particles which track the helium plume. Light from a 10 Hz pulsed Nd:YAG laser, frequency quadrupled to 266 nm, is formed into a sheet roughly 1 mm above the duct exit. Light scattered by the particles is imaged onto the detector of a UV sensitive, intensified video camera, and digitized by a PC and frame grabber. Sequences of 150 images were typically acquired. Images were not synchronized to the phase of injection, but were acquired at random phase, minimizing the amount of data acquired in this preliminary experiment.

The images of the duct exit flow were distorted because the camera viewed the flow obliquely through a mirror located just outside the jet formed by the flow exiting the duct. This distortion was corrected by bilinear interpolation with reference to an image of a grid placed at the duct exit plane.

The light scattered from the particles could not easily be related to the helium number density, since scattering intensity does not depend in a simple way on ethanol concentration. Rather, it is proportional to the number of particles and particle diameter to the $4^{th}$ power. Particle size distribution varies and may depend on the condensation process, which may in turn be effected by unsteady injection. Thus, sequences of digital images of scattered light were analyzed in a manner that was as independent of particle diameter as possible. Each pixel of a digital image has a "value" or number of counts associated with it, corresponding to light intensity. For each image, a histogram of values was formed, and the value at the peak, $N_0$, i.e., the most frequently occurring value, was found. It was observed that almost all pixels that were unambiguously in the freestream (i.e., outside the helium plume) had values below $N_0 + 3$. The average value of all the pixels whose value falls above $N_0 + 3$, $N_1$, was found. A "new" threshold value, $N_2 = N_0 + K(N_1 - N_0)$, was found, where $K$ is a constant. Regions of the image with pixel value above $N_2$ were then identified with the plume by resetting their pixel values to 1, while the regions with pixel values below the threshold were set to 0. This identified areas that were unambiguously part of the helium plume in a manner consistent from image to image, independent of variations in laser energy level, ethanol concentration in the helium supply, and camera intensifier gain setting. This procedure was repeated for each image of a sequence, and the average and standard deviation of the area of the plume were obtained.

## RESULTS

### Injector Development

The initial configuration (Figure 3) utilized Insert 1, which had a constant area inlet passage, and Wheel 1, which was square. Lacking design rules, it was designed for geometric simplicity. Figure 4 shows a plot of frequency as a function of pressure with air, helium, and a mixture of 95% helium/5% air by volume. It is believed that at pressure ratios above 2-2.5 the flow in the nozzle formed between the insert and the wheel is sonic. Below this pressure, frequency behaves erratically, while above it, $f/a^*$ rises smoothly to an asymptote of about 2.2. Results collapse for the different gases. This frequency is much less than required in the present study, so that further inserts and wheels were designed and tested.

Inserts 5, 6, and 7 (Figure 5) were designed so that flow from the inlet passage is accelerated through a fixed nozzle to form a jet that impinges upon the wheel. During rotational phases where the throat formed between insert and wheel is less than average, some of the jet fluid is deflected into the "vortex plenum". During rotational phases when the throat is greater than average, both jet and plenum fluid are discharged from the device. Much higher frequencies were obtained with this type of insert, due (presumably) to much higher impingement velocities upon the wheel. Insert 6 was designed so that, by comparison with Insert 5, the effect of vortex plenum size could be found. Insert 7 was designed so that, by comparison with Insert 6, the effect of fixed nozzle throat size could be found. Since it was not possible to manufacture a large number of additional wheels for testing, due to cost, Wheel 3 was designed both to be 3-sided and to have hooked corners

while maintaining roughly the same average (throat) area between insert and wheel over a rotation cycle as Wheel 1.

Figure 6 shows plots of frequency for Insert 5, Wheel 1, with air and helium: $f/a^*$ rises rapidly with pressure ratio, to an asymptote of about 7.5. Since the pressure moments on the wheel must exactly balance (neglecting friction), the asymptotic condition is a condition for which the pressure distribution around the wheel (made dimensionless with inlet pressure) becomes independent of inlet pressure. This condition is consistent with choked flow at the throat between insert and wheel. In addition, results are generally independent of $\gamma$, which differs between air and helium.

Figure 7 shows plots of $f/a^*$ for Inserts 5, 6, 7 and Wheels 1, 3 for air. Results for Wheel 1 are similar to each other. The effect of replacing Wheel 1 with Wheel 3 depends on insert, with little effect for Insert 1, an increase in asymptotic $f/a^*$ to about 11 for Insert 6, and to about 15 for Insert 7.

The reasons for the greater pulsation frequency obtained with Wheel 3 are not fully understood. Some clues however may be found by considering the surface flow and pressure time histories in the vortex plenum.

A photograph of vortex plenum surface flow for Insert 6, Wheel 1 (Figure 8) shows a well-defined spiral pattern. While surface flow lines do not necessarily follow streamlines away from the surface, the results indicate the presence of a relatively steady rotating flow in the vortex plenum. No such well-defined structure could be obtained in the Wheel 3 cases, suggesting an unsteady flow without dominant rotation.

Figure 9 shows a typical vortex plenum pressure time-history for Insert 7, Wheels 1 and 3. Time is made dimensionless with the independently measured pulsation period. A third line shows the sonic pressure. Figure 10 shows the power spectral density (psd) of the pressure histories. With Wheel 1, the pressure varies roughly sinusoidally about the sonic pressure as the vortex plenum gains then loses mass in a cycle. There is a single and well-defined peak in the psd at the pulsation frequency ($f\tau$=1). With Wheel 3, pressure levels are generally lower and the pressure cycle is multi-peaked but repeatable. The psd has its largest peak at the 2nd harmonic ($f\tau$=2), and significant peaks occur at several other harmonics. That the peaks occur at harmonics indicates only that the waveform is periodic. However, the large size of the 2nd harmonic with Wheel 3 indicates that wave processes are important in this case. The time found by dividing twice the length of the vortex plenum by the speed of sound in the plenum is roughly half the period of the 2nd harmonic. Thus, a compression wave generated as the throat formed between the insert and wheel is closed travels the length of the vortex plenum and back in the time it takes for the throat to open. This behavior may not be a coincidence, i.e., with Wheel 3 the injector may somehow select such a frequency.

Plots of injector sonic area as a function of pressure are shown in Figure 11 for Inserts 6 and 7 with no wheel, Wheel 1, and Wheel 3. The sonic area is non-dimensionalized with the area of the fixed nozzle throat. If all the flow entering the injector passes isentropically through the fixed nozzle, and is 1-D sonic at the throat (choked), $A^*/A_{throat}$=1. In all cases, $A^*$ is nearly constant over the range of inlet pressures considered, indicating that the injector as a whole is choked (although the fixed nozzle may not be). Since, with no wheel, the fixed nozzle provides the only throat, the fixed nozzle must be choked in these cases. With both inserts, $A^*/A_{throat}$ is slightly greater than 1.0, presumably because some (leakage) flow bypasses the fixed nozzle throat (the injector assembly used no O-rings or gaskets). With Insert 7, $A^*$ is the same with or without wheels, i.e., the fixed nozzle is always choked. However, with Insert 6, $A^*$ is reduced by the wheels, indicating that the flow in the fixed nozzle is not choked (at least for some portion of the injection cycle) in these cases. Note that choking of the flow in the fixed nozzle does not preclude the possibility the flow in the throat between insert and wheel also chokes. The lower pulsation rates obtained with Insert 6/Wheel 3 than with Insert 7/Wheel 3 may possibly be explained by the lower velocity of the jet impacting the wheel.

Finally, Figure 12 shows schlieren images of the flow at the exit of the injector for a single case: Insert 7, Wheel 3, $p_t/p_{exit}$=18.3. The purpose is to provide visual evidence that these injectors indeed generate high-speed pulsed jets. Additional results for other cases are given in Reference 13. The images correspond to various phases of the injection cycle, as indicated by the superimposed line drawings of the insert and wheel. Injection is initiated at $t$=0. At $t$=60 μs turbulent flow may be seen exiting the injector, and as many as three shock waves, visible as dark and light vertical bands, are located within about 0.015 m of the exit (dark indicates increasing density from right to left). At $t$=120 μs and $t$=180 μs, the turbulent jet is seen to extend to the right, and the waves radiate away from the nozzle exit. By inspection of these images, the turbulent leading edge of the jet is found to move away from the nozzle exit at about Mach 1. Since the leading edge is

not expected to move as fast as the flow exiting the injector, due to mixing, the flow exiting the injector must be supersonic over some portions of the injection cycle.

Injection into Crossflow

Figures 13 and 14 show schlieren images for $p_t/p_{duct}$=16.4 and 32.7 respectively. The top four images in each figure are for Insert 1 Wheel 1 at various times in the injection cycle, with the 1st image at the nominal start of injection. The bottom image is with no wheel. The height of each image exactly matches the height ($h$) of the duct, injection is from the top left, and flow is from left to right. Each image shows the bow shock, visible as the sharp edge of a curved band of white extending from top left to bottom right. The helium plume is visible as a ragged turbulent region downstream of the shock, toward the top. In each case, the bow shock undergoes the following evolution during a cycle. At $t$ = 50 μs an oblique shock has formed in the vicinity of the injector as injection starts, which steepens at $t$ = 100 μs and 150 μs (injection ends). At $t$ = 0 the shock "bubble" begins to convect downstream, and then the cycle repeats. Shock angles are generally steeper in the higher-pressure cases, and additional shock structures are visible in the bottom right quadrant. It is believed these occur near the end walls of the duct due to shock-induced separations.

Figures 15-17 are (randomly) selected helium plume images at the duct exit plane with Insert 7, and, respectively, no wheel, Wheel 1, and Wheel 3. All images are for $p_t/p_{duct}$=32.7. Dark represents large scattered intensity, and the solid lines top and bottom of the images show the locations of the duct walls. Injection is from the bottom wall. In all cases there is great variability from image to image. With no wheel, the variability is the least, and each image shows some resemblance to a "mushroom cloud", evidence of a counterrotating vortex pair. With Wheel 1, the variability is the greatest, and the plume the most ragged. In some images large portions of the plume appear smeared along the opposite wall, and in others the plume is nearer the injection wall. There is no consistent resemblance to a mushroom cloud. With Wheel 3 the plume appears a little smaller, with image-to-image variability intermediate between the previous cases.

Figure 18 shows the images of Figure 16 after being thresholded using $K$=0.5. Regions of the image assigned to the plume (given pixel value 1) are shown as black. Figures 19 and 20 show the mean and standard deviation of the area of the plume (i.e., of the black region), made dimensionless by duct height squared, for all cases. Since the choice of $K$ was arbitrary, values of $K$ of 0.25, 0.5, and 0.75 were used. While the choice of $K$ affects the area, it does not affect the trends between cases. For given injector inlet pressure, the plume area appears to decrease in going from the no wheel case to Wheel 1 to Wheel 3. Given that an equal mass rate of helium is injected, a reduction in plume area suggests that the plume has entrained less air, i.e., the mixing is less. The standard deviation of plume area is least for the no wheel case, greatest for Wheel 1, and intermediate for Wheel 3, indicating greatest unsteadiness with Wheel 1. This is consistent with previous observation.

## CONCLUSIONS

An injector has been developed to provide high-frequency supersonic pulsed jet. The injector nozzle is formed between the fixed internal surface of the nozzle and a freely rotating 3- or 4-sided wheel embedded within the device. Pulsation frequency is proportional to the speed of sound in the injected gas. A wide range of pulsation frequencies could be obtained by selection of nozzle internal flow passage and wheel shape. Higher frequencies were obtained when the internal flow passage contained a fixed nozzle and plenum ahead of the wheel. Higher frequencies were also obtained with 3-sided, hooked wheel.

A preliminary investigation was conducted of the effects of pulsed injection of helium into a Mach 1.98 crossflow of (unheated) air. A "target" frequency of 13.3 kHz was identified around which (both above and below) injection is expected to have a significant effect on mixing. Three cases were considered: steady injection, and pulsed injection at 4.6/5.1 kHz and 11.8/12.8 kHz. The helium plume was imaged in a plane normal to the flow at the duct exit. Plume cross sectional area was slightly reduced by pulsed injection (the more so at the higher frequency), and plume unsteadiness increased (the more so at the lower frequency). These conclusions must be regarded as preliminary, due to the uncertain nature of the flow visualization technique and to the inability to probe the higher frequencies of interest.

## ACKNOWLEDGEMENTS

The 1st and 2nd authors would like to acknowledge the support of the NASA Langley Research Center through grant NCC1-370.

## REFERENCES


[1] Yu, K. H., Schadow, K. C., "Cavity-Actuated Supersonic Mixing and Combustion Control," *Combustion and Flame*, Vol. 99, pp. 295-301, 1994.

[2] Sato, N., Imamura, R., Shiba, S., Takahashi, S., Tsue, M., Kono, M., "Advanced Mixing Control in Supersonic Airstream with a Wall-Mounted Cavity," AIAA Paper 96-4510-CP, 1996.

[3] Wood, C. W., Thomas, R. H., Schetz, J. A., "Effects of Oscillating Shock Impingement on the Mixing of a Gaseous Jet in a Mach 3 Airstream," AIAA Paper 90-1982, July 1990.

[4] Wood, C., Schetz, J., "Effects of Unsteady Shock Impingement on High-Speed Gaseous Mixing," AIAA Paper 91-5091, Dec. 1991.

[5] Kraus, D. K., Cutler, A. D., "Mixing of Swirling Jets in a Supersonic Duct Flow," *Journal of Propulsion and Power*, Vol. 12, No. 1, 1995, pp. 170-177.

[6] Doerner, S. E., Cutler, A. D., "Effects of Jet Swirl on Mixing of a Light Gas Jet in a Supersonic Airstream," NASA / CR-1999-209842, Dec. 1999.

[7] Cutler, A. D., Doerner, S. E., "Effects of Swirl and Skew upon Mixing of Supersonic Wall Jets in Crossflow," accepted for publication, *Journal of Propulsion and Power*.

[8] Bogdanoff, D. W., "Advanced Injection and Mixing Techniques for Scramjet Combustors," *Journal of Propulsion and Power*, Vol. 10, No. 2, 1994.

[9] Seiner, J. M., Dash, S. M., Kenzakowski, D. C., "Historical Survey on Enhanced Mixing in Scramjet Engines," AIAA Paper 99-4869, Nov. 1999.

[10] Vermeulen, P. J., Chin, C.-F., Yu, W. K., "Mixing of an Acoustically Pulsed Air Jet with a Confined Crossflow," *Journal of Propulsion*, Vol. 6, No. 6, 1990, pp. 777-783.

[11] Hornung, H., "Vorticity Generation and Transport," Paper KS-3, 10th Australasian Fluid Mechanics Conference - University of Melbourne, 11-15 Dec. 1989.

[12] Vakili, A. D., Chang, Y. K., Wu, J. M., "Supersonic Mixing Enhancement Using Pulsed Transverse Fuel Jets," The University of Tennessee Space Institute, Final Report for ONR Grant Navy N00145-89-J-1696, Aug. 1995.

[13] Harding, G. C., "Development of a High-Frequency Supersonic Pulsed Injector," MS Thesis, The George Washington University, School of Engineering and Applied Science, Dec. 2000.


## FIGURES

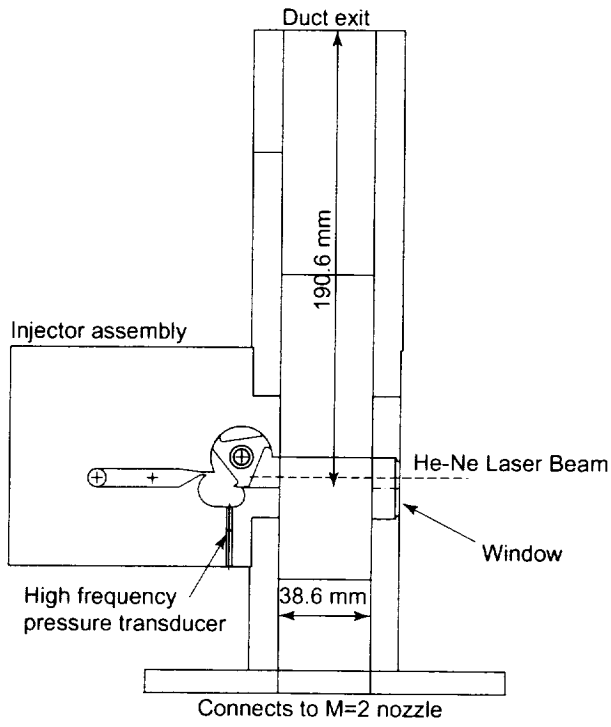


**Figure 1 Injector installed in duct.**

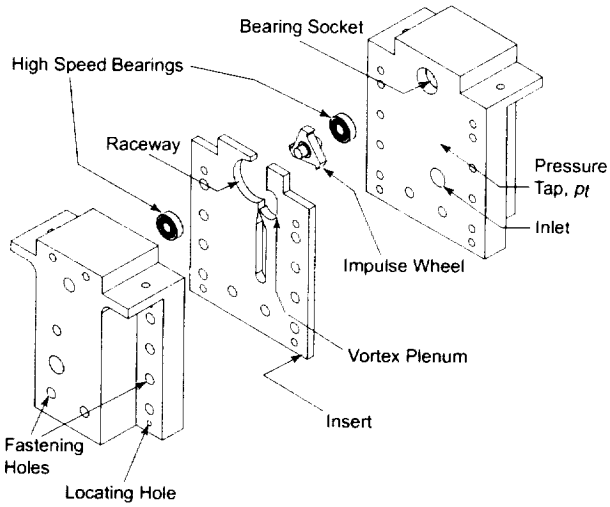


**Figure 2 Isometric view of injector assembly.**

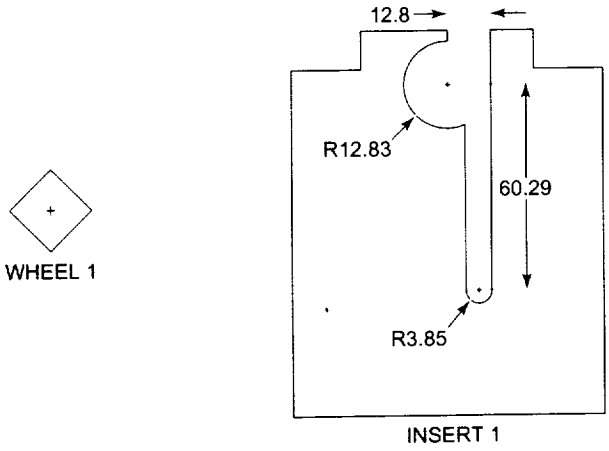


**Figure 3 Insert 1 and Wheel 1 (dimensions in mm).**

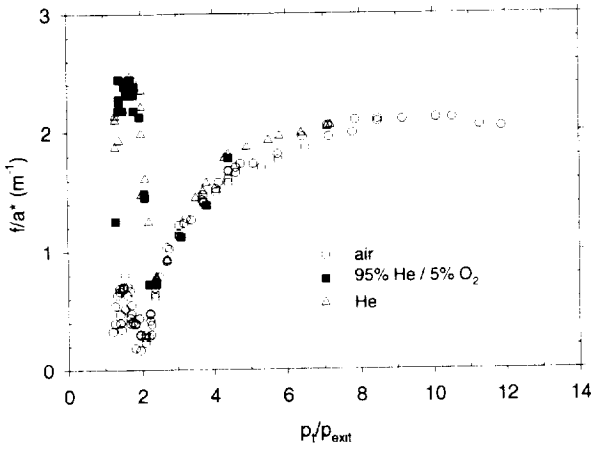


**Figure 4 Pulsation frequencies for Insert 1, Wheel 1.**

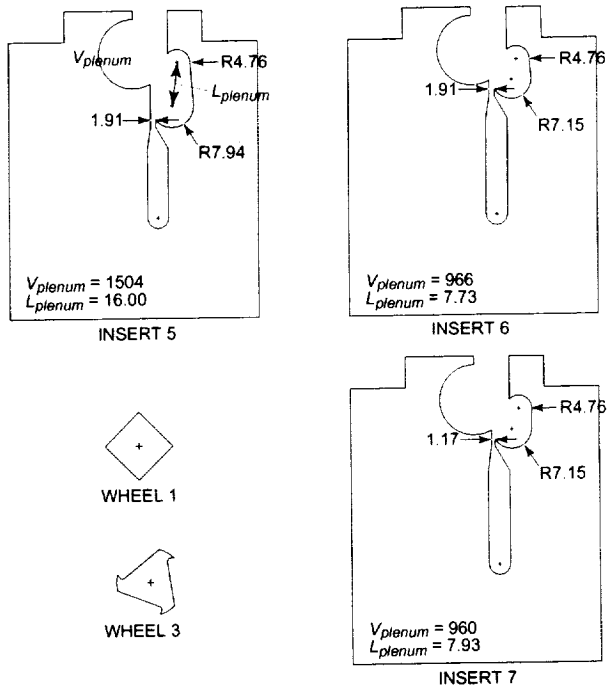


**Figure 5 Vortex plenum inserts and wheels (dimensions in mm).**

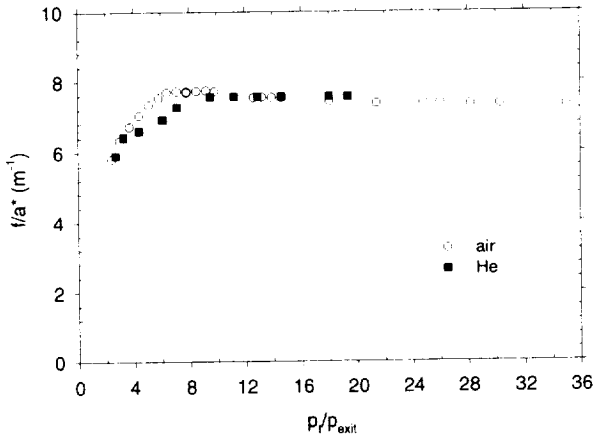


**Figure 6 Pulsation frequencies for Insert 5, Wheel 1.**

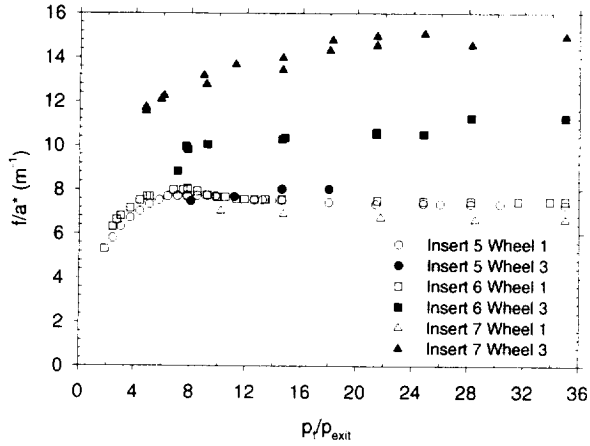


**Figure 7 Pulsation frequencies for vortex-plenum inserts, air.**

**Figure 8 Vortex plenum surface flow, Insert 6, Wheel 1.**

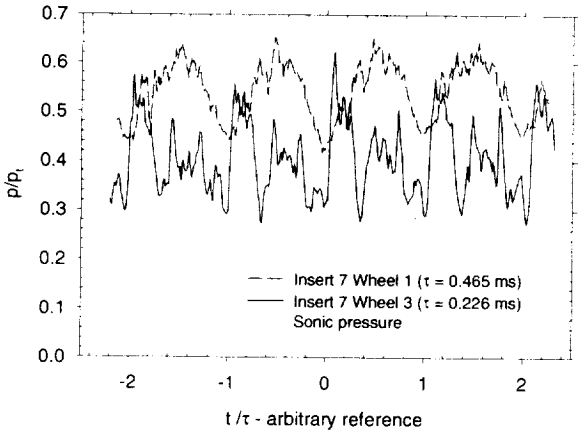


**Figure 9 Vortex plenum pressure time history, $p_t/p_{exit}$=18, air.**

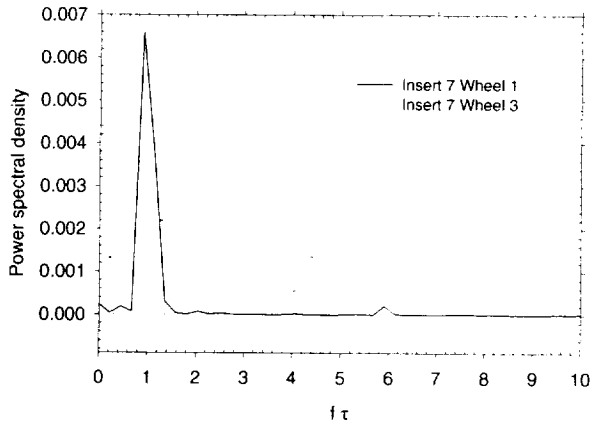


**Figure 10 Power spectral density of vortex plenum pressure time histories.**

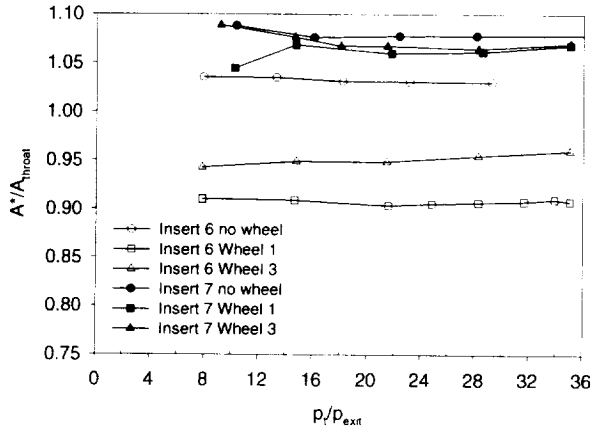


**Figure 11 Equivalent sonic-throat-areas of vortex-plenum inserts, air.**

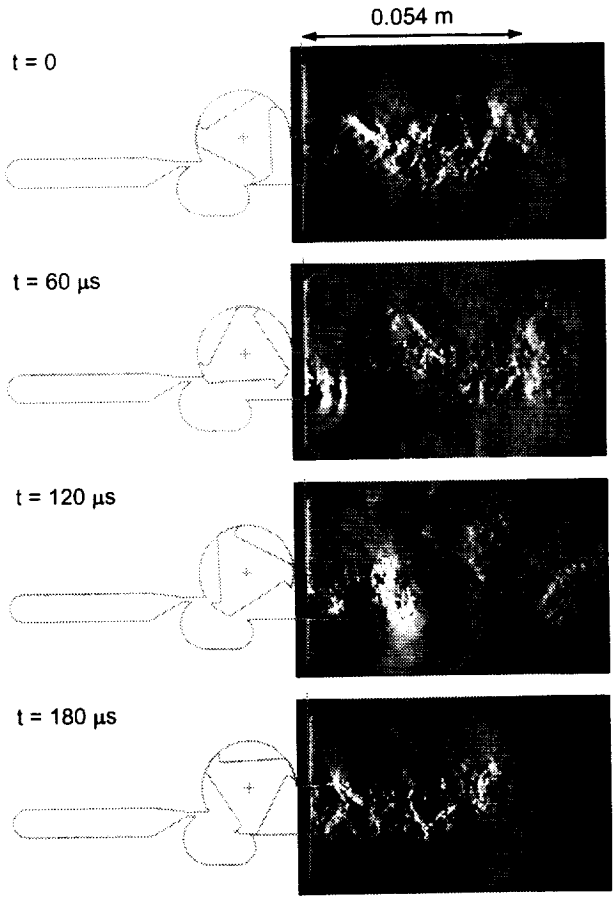


**Figure 12 Schlieren for injection of air into stagnant air: Insert 7, Wheel 3, $p_t/p_{exit}$ = 18.3, $\tau$ = 223 μs.**

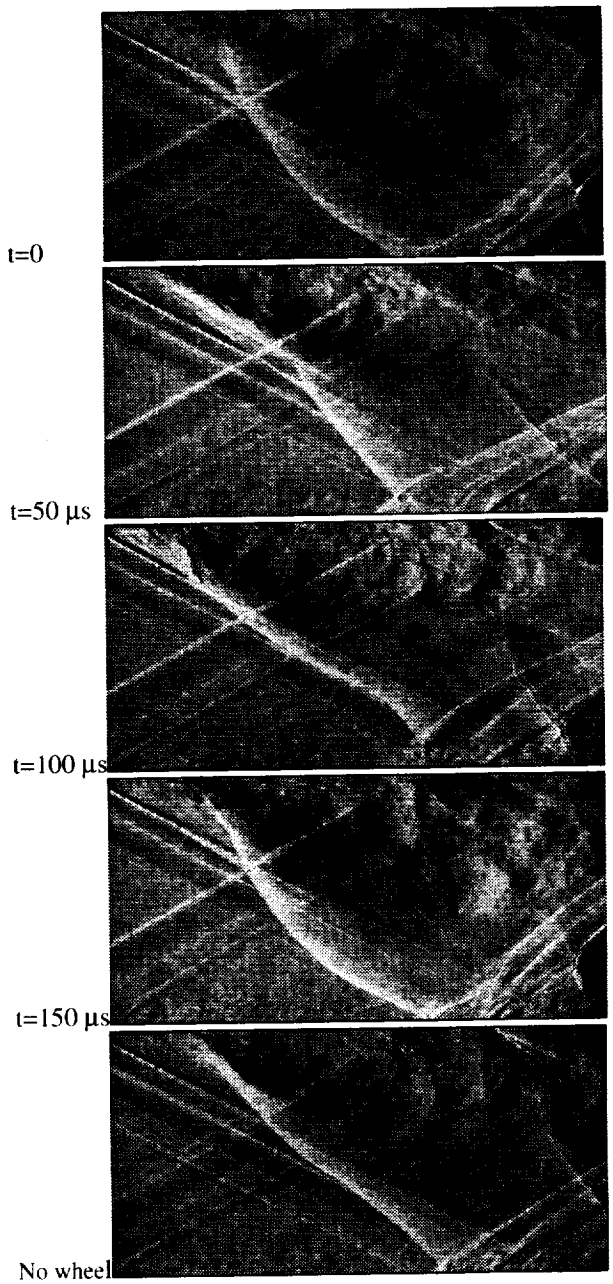


**Figure 13 Schlieren images of injection of helium into a supersonic duct flow, Insert 7, Wheel 1, $p_t/p_{duct}$=16.4, $\tau$=217 μs.**

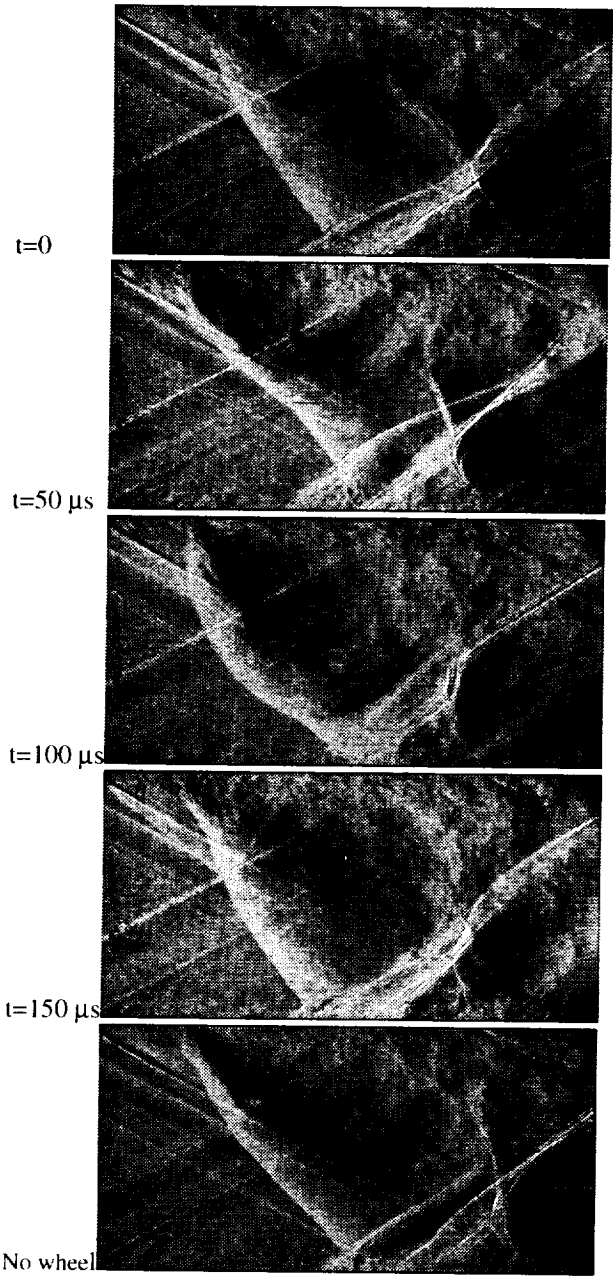


**Figure 14 Schlieren images of injection of helium into a supersonic duct flow, Insert 7, Wheel 1, $p_t/p_{duct}$=32.7, $\tau$=196 μs.**

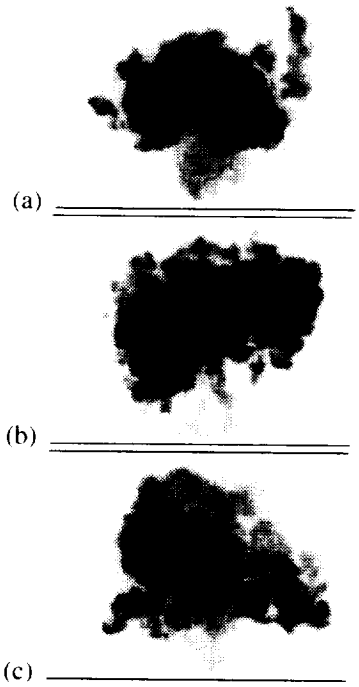


**Figure 15 Selected plume images, Insert 7, no wheel, $p_t/p_{duct}$=32.7.**

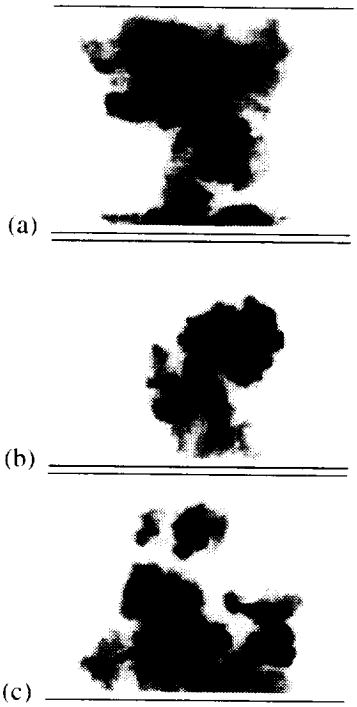


**Figure 16 Selected plume images, Insert 7, Wheel 1, $p_t/p_{duct}$=32.7.**

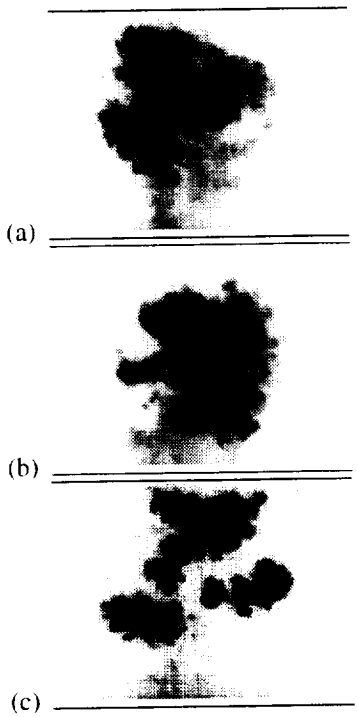


**Figure 17 Selected plume images, Insert 7, Wheel 3, $p_t/p_{duct}$=32.7.**

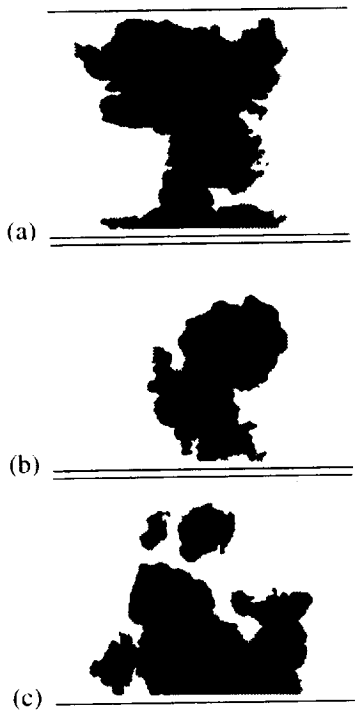


**Figure 18 Thresholded images ($K$=0.5) corresponding to Figure 16.**

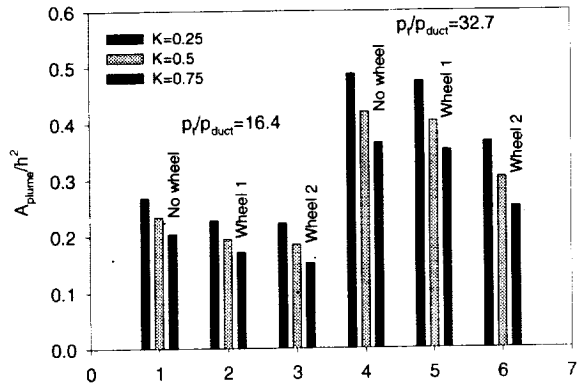


**Figure 19 Average of plume area for various threshold levels, Insert 7.**

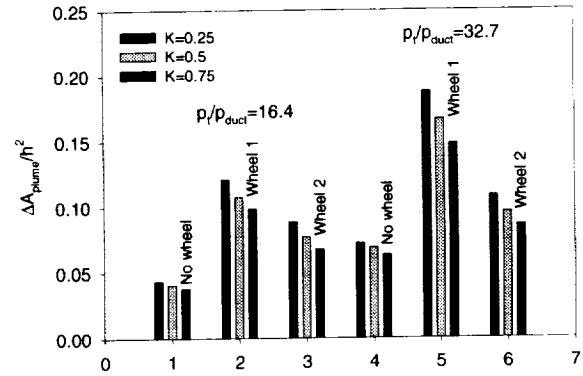


**Figure 20 Standard deviation of plume area for various threshold levels, Insert 7.**